Numerical calculation on a two-Step subdiffusion behavior of lateral protein movement in plasma membranes

Tomonari Sumi,[1,2,a] Atsushi Okumoto,[3] Hitoshi Goto,[3] and Hideo Sekino[3,4]

[1]*Research Institute for Interdisciplinary Science and* [2]*Department of Chemistry, Faculty of Science, Okayama University, 3-1-1 Tsushima-Naka, Kita-ku, Okayama 700-8530, Japan*

[3]*Department of Computer Science and Engineering, Toyohashi University of Technology, Tempaku-cho, Toyohashi 441-8580, Japan*

[4]*Institute for Advanced Computational Science, Stony Brook University, Stony Brook, NY 11794, USA*

A two-step subdiffusion behavior of lateral movement of transmembrane proteins in plasma membranes has been observed by using single-molecule experiments. A nested double-compartment model where large compartments are divided into several smaller ones has been proposed in order to explain this observation. These compartments are considered to be delimited by membrane-skeleton "fences" and membrane-protein "pickets" bound to the fences. We performed numerical simulations of a master equation using a simple two-dimensional lattice model to investigate the heterogeneous diffusion dynamics behavior of transmembrane proteins within plasma membranes. We show that the experimentally observed two-step subdiffusion process can be described using fence and picket models combined with decreased local diffusivity of transmembrane proteins in the vicinity of the pickets. This allows us to explain the two-step subdiffusion behavior without explicitly introducing nested double compartments.

I. Introduction

Nearly half a century ago, Singer and Nicolson proposed that the fluid mosaic model could be applied as the basic structure of cell membranes[1]. It was subsequently found that transmembrane proteins and lipids do not immediately undergo a steady-state normal diffusion process within plasma membranes. Furthermore, the lateral diffusion coefficient

[a]Author to whom correspondence should be addressed. Electronic mail: sumi@okayama-u.ac.jp

of these molecules in plasma membranes was found to be between 5 and 50 times lower than that observed in artificial reconstituted membranes[2-9]. The mechanism that was responsible for the reduction in the lateral diffusion would be attributable to structural and dynamical heterogeneities of plasma membranes. However, higher-order organization structures of plasma membranes were required to explain these heterogeneities, because such long-ranged structures do not exist in the reconstructed membranes consisted of membrane proteins, lipids, and cholesterol molecules under physiological concentrations. As a possible origin of the heterogeneity in plasma membranes, effects of membrane cytoskeletons on the lateral diffusion of transmembrane proteins (TMP) had been experimentally demonstrated by varying the membrane cytoskeleton components in erythrocyte membranes. [2,10-12] On the basis of these experimental observations, a corral model, which is formed by the membrane cytoskeletons near the plasma membrane surface, was proposed. [2,10-13]

Fujiwara *et al.* investigated the physical origin responsible for the significant slowing of the lateral diffusion by using both single-fluorescent-molecule video imaging and single-particle tracking [14]. They found as follows: both an unsaturated phospholipid, 1,2-dioleoyl-sn-glycero-3-phosphorylethanolamine (DOPE), and a transmembrane protein, the transferrin receptor (TfR), in normal rat kidney (NRK) fibroblastic cells was confined by small and large compartments (with 200 and 700 nm on average, respectively); after a while these molecules underwent hop diffusion among adjacent compartments. They also demonstrated that the membrane cytoskeletons were primarily responsible for such temporary confinements of not only TfR but also DOPE. That effect of membrane cytoskeletons on the lateral diffusion of DOPE was unexpected because DOPE was located in the outside of the membranes and thus do not directly interact with the cytoskeletons. On the basis of these observations, they proposed an anchored membrane-protein “picket” model (see Fig. 1); in this model, various membrane proteins bound to the actin-based membrane cytoskeleton act as pickets.

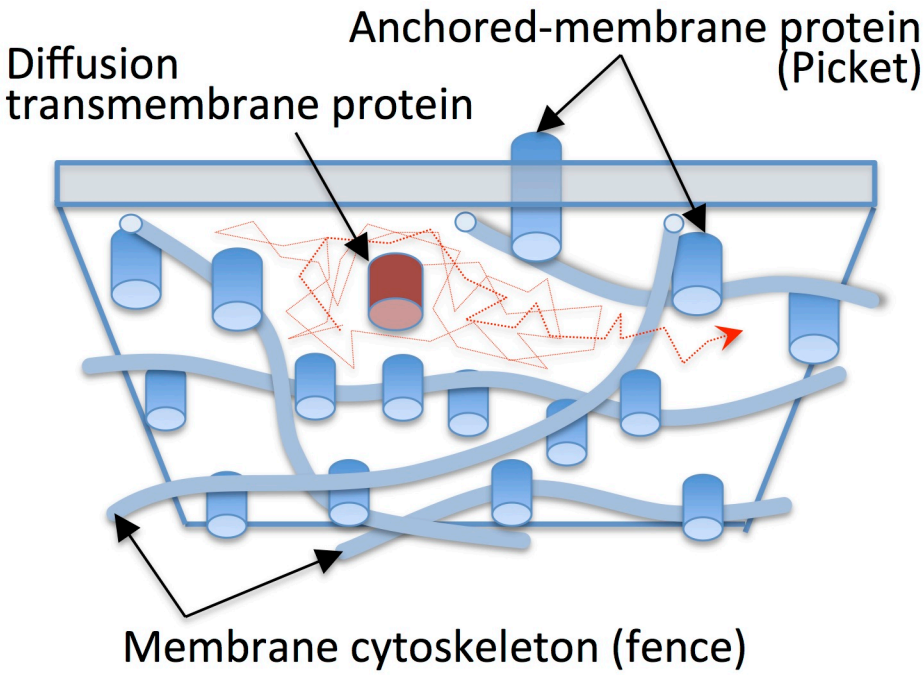

Figure 1. The membrane-cytoskeleton "fence" model and anchored membrane-protein "picket" model that are responsible for the compartmentalization on the lateral diffusion of transmembrane proteins (TMPs) in plasma membranes[14]. A TMP molecule is temporarily corralled by both the membrane-cytoskeleton fences and anchored-protein pickets before undergoing hop diffusion from one compartment to an adjacent one. The TMP is confined within compartments formed by the actin-based membrane cytoskeletons, because it protrudes into the cytoplasm and its cytoplasmic domain collides with the membrane cytoskeletons. Various membrane proteins are anchored to the actin-based cytoskeletons. The membrane proteins bound to the cytoskeletons effectively act as pickets hinder the lateral diffusive movement of not only TMPs but also lipids (not shown in Fig. 1) in the plasma membranes.

A large difference between the compartmental residency times of DOPE and TfR within compartments (13 and 65 ms, respectively) has been experimentally observed. The difference can be explained by considering an effect of the membrane cytoskeletons on only the TfR in addition to the effects of the picket obstacles on both the DOPE and TfR. Since the cytoplasmic domain of the TfR collides with the membrane cytoskeletons, the TfR is temporary corralled by the membrane-cytoskeleton meshes[15-18]. This additional mechanism to TMPs is called the membrane-skeleton "fence"

model (see Fig. 1). Fujiwara *et al.* also demonstrated that, in addition to the diffusive movement of both the DOPE and TfR that were confined by compartments with diameters evaluated to be about 700 nm on average [16,17], hop diffusion of the DOPE and TfR among smaller compartments (that had the diameter of about 200 nm on average) was more clearly observed than that among the 700-nm large compartments [14]. Furthermore, Suzuki *et al.* observed a two-step subdiffuion behavior of a G-protein coupled receptor called an μ-opioid receptor (μOR) in NRK cell membranes [19]. In order to explain these experimental observations, a nested double compartment model, in which the large compartments are divided into several smaller ones, has been proposed by them [14,19]. In our preliminary Monte Carlo simulations, we found that a similar two-step subdiffusion behavior could be described by using a nested double compartment model, if the picket obstacles were added with a high coverage along every three rows and three columns of the fences. However, this model with such inhomogeneous distribution of the pickets cannot simultaneously describe the confinement of lipid molecules within the small compartment experimentally observed by Fujiwara *et al*. [14]; it is because, the lateral movement of lipid molecules is affected by only the three times larger compartment formed by the non-uniformly distributed pickets. Thus, such a model with the non-uniformly distributed pickets is not a candidate of the model for the NRK cell membranes. Conversely, the fence and picket models such that the pickets are randomly distributed along all the fences allows for no more than a simple single-step subdiffusion process to be described. To model nested double compartments consisted of the small and large compartments, two different boundaries forming the small and large ones are needed. In fact, if we assumed that a barrier for the large compartments was higher than that for the smaller compartments, as pointed out by Fujiwara *et al*. [14], the two-step subdiffusion behavior would be described by the

nested-double compartment model. However, it has been remained unclear how the molecular origin of these different boundaries is explained according to the membrane-skeleton fences and anchored-membrane-protein pickets.

In order to investigate lateral diffusion behaviors of lipid molecules and TMPs in plasma membranes, a lot of computer simulations[20-31] and theoretical studies[32-36] have been conducted. Most of these studies examined the effects of obstacles and/or traps on lateral diffusion caused by membrane cytoskeletons and/or anchored membrane proteins[24,32,33,36] or focused on simple subdiffusion behaviors from anomalous diffusion to normal diffusion.[20-23,25-29,31,34,35] In contrast, the two-step subdiffusion behavior on the diffusive movement of the TMP observed in NRK cell membranes by Suzuki *et al.* [19] has only been investigated by one computer simulation study.[30] In the present study, in order to investigate the physical origin of the two-step subdiffusion behavior and gain insight into the heterogeneous structure and dynamics in the plasma membranes, we perform numerical simulations of a master equation using simple two-dimensional lattice models. In our model, explicit nested double compartments by two different boundaries is not assumed; instead, in addition to the obstacle effects on the TMP's diffusion caused by the stochastic fences and immobilized pickets, a reduction in the local diffusivity of the TMP around the pickets is taken into account. The reduction in the local diffusivity could be explained by an increase in the local viscous friction due to a reduction in the local diffusive movement of lipid molecules around the membrane-protein pickets. Indeed, the significant reduction in the diffusive movement of phospholipid molecules has been observed at the axonal initial segment in plasma membranes of developing hippocampal neurons in culture, wherein various membrane-protein pickets

are accumulated by binding to the dense membrane-skeleton meshes [37]. Our simple model can quantitatively describe the two-step subdiffusion behavior, and it thus allows us not only to examine the effects of the fence and picket on the transient process of the TMP diffusion, but also to clarify how the reduction in the local diffusivity of the TMP around the pickets affect the two-step subdiffusion behavior. The results imply that the explicit nested double compartmentalization is not necessarily needed to explain the experimentally observed two-step subdiffusion behavior of the TMP.

The paper is organized as follows: the two-dimensional lattice model for the plasma membranes is presented in Section II. The details of the numerical calculations on the master equation are given in Section III. The results and discussions are provided in Sections VI and V, respectively. Lastly, the paper is summarized in Section VI. The derivation of the master equation for the diffusion equation of TMP in an inhomogeneous medium is presented in APPENDIX.

II. Model

We used a two-dimensional lattice model to perform numerical simulations for the diffusion process of the TMP in the plasma membranes (see Fig. 2). The TMPs generally protrude into the cytoplasm, and their cytoplasmic domains collide with membrane cytoskeletons; this means that they are temporarily corralled not only by the anchored-protein pickets, but also by the membrane-skeleton fences. The TMPs, after a while, undergo hop diffusion from one compartment to an adjacent one. Based on the images in Fig. 2, we modeled the membrane-skeleton fences as immobile obstacles (they are

depicted as the blue square sites in Fig. 2). These obstacles are placed in a grid that has equally spaced vertical and horizontal lines. The fence obstacle is randomly replaced to be vacant site (indicated as yellow in Fig. 2) with a probability p_v every step, and they become fence obstacles again at the next step. The fences acting as dynamical obstacles allow the stochastic passage of the TMP across the fences, which is induced by the thermal fluctuations of the plasma membrane. Thus, p_v can be related to the passage probability of the TMP across the fences. The anchored membrane-protein pickets are modeled as immobile obstacles (they are indicated as the green square sites in Fig. 2) that are randomly assigned by a probability p_p at the beginning of the simulation. The picket obstacle is never replaced by vacant site during the simulation so that it always acts as the immobile obstacle. p_p qualitatively corresponds to the concentration of pickets bound to the membrane-skeleton fences. The reduction in the local diffusion coefficient of the TMP is taken into account at the nine sites surrounding each picket including the picket sites (in part indicated by the light-red panels in Fig. 2); this is done by multiplying the free diffusion coefficient, D_0, by a factor, R_d. Noted that the area with the reduced local diffusion coefficient of the TMP is fixed during the simulation, because the pickets are also fixed after they have been randomly assigned at the start of the simulation.

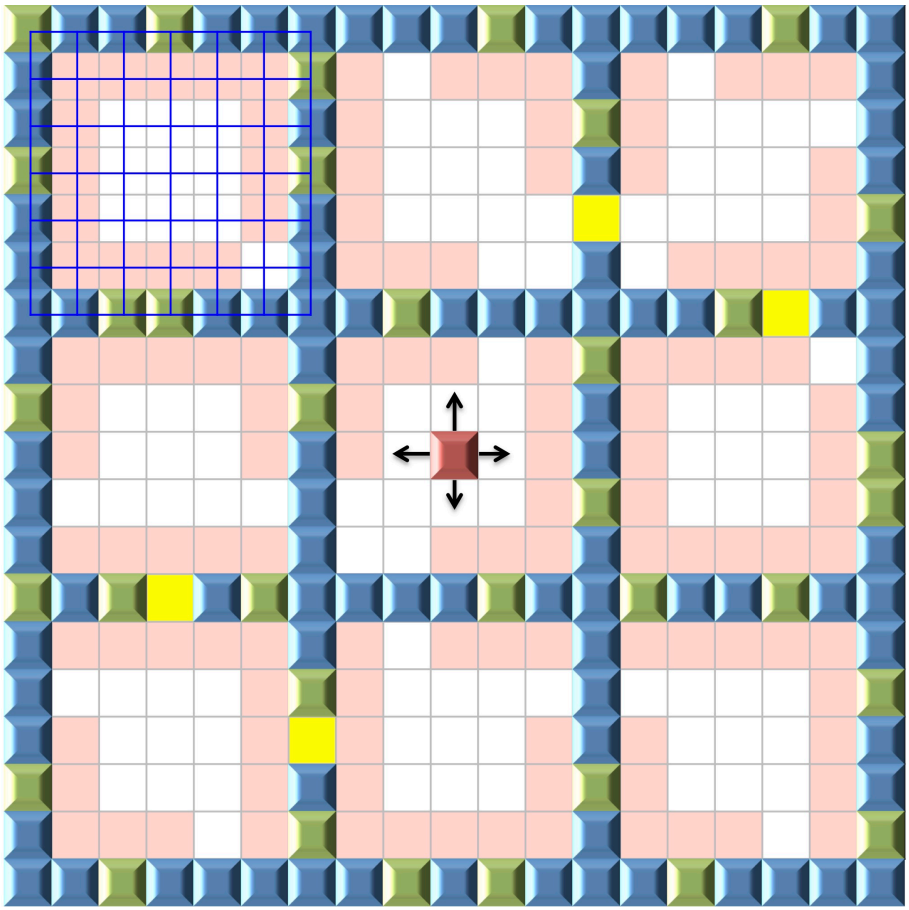

Figure 2. A two-dimensional lattice model on the lateral diffusion process of the TMPs (red square site) in the plasma membranes based on the membrane-skeleton fences (blue square sites) and the anchored-protein pickets (green square sites). It is noted that the blue lines on the left upper side of this figure show the actual lattice points. Vacant sites (indicated as yellow) are randomly chosen among the fence obstacles by a constant probability every step, and they become fence obstacles again at the next step; this is done in order to account for the stochastic passage of the TMP across the fences. The green sites are never chosen as vacant sites, because they act as the pickets that are anchored to the membrane cytoskeletons. The nine sites surrounding the pickets including the picket sites, which in part are indicated as the light-red panels, correspond to the areas in which the local diffusion coefficient of the TMP is reduced.

III. Computational Details

We used a 5,000-square lattice with spacing between the fences of $L_f = 6$. We made a direct comparison of the numerical results of $\langle r^2(t)\rangle/t$ with the single-molecule experimental data for the μOR in NRK cell membranes provided by Suzuki *et al.*[19] They estimated that the small and large compartments had average diameters of 210 and 730 nm,

respectively. In the Monte Carlo simulation study by Sung and Yethiraj [30], the fence effect was assumed to describe the large compartment of 730 nm. We examined the cases using both 210 and 730 nm as the spacing between the fences, and we found that the first subdiffusion process could not be described by using our model with 730-nm spacing between the fences. Therefore, we assigned the compartments divided by the fences to the small 210-nm compartments that have been more clearly observed than the large compartments by the single-molecule experiments [14,19]. In the case of $L_f = 6$, we determined that the spacing between lattice points Δx and Δy was 210 nm/L_f = 35 nm. The time step, Δt, was provided by $\Delta t = \Delta x^2/5D_0$ using the free diffusion coefficient D_0 of the TMP observed in the NRK cell membrane inside each compartment. The starting position of the diffusion TMP, (x_0, y_0), was chosen to be the center of the compartment (Fig. 2) that was located at the center of the square lattice. This resulted in the probability at time $t = 0$, $P(x, y, t = 0)$, being 1 at the starting position (x_0, y_0) and 0 at all other lattice points.

The probability p_v of randomly replacing the fence obstacles with vacant sites, which is related to the passage probability of the TMP across the fences, was examined for 0 (completely confined within the initial compartment), 0.0005, 0.001, 0.002, 0.004, 0.006, 0.01, 0.1, and 1 (no fence effect). The probability p_p of randomly choosing an immobile picket site among the fence obstacles was examined for 0 (no pickets), 0.1, 0.2, 0.3, 0.4, and 0.5. The size of immobile picket site was obtained to be 35 nm in the case of $L_f = 6$ since each site indicated as green square panel was randomly assigned to be as an immobile picket domain as shown in Fig. 2. This value was more than ten times larger than the diameter of transmembrane proteins, implying that it should rather be regarded as domains where

transmembrane proteins were bound by a high concentration to the membrane-skeleton fences. As for the reduction in the local diffusive movement of the TMP around the pickets, we assigned the nine sites surrounding each picket including its site to the area, which in part is indicated by the light-red panels in Fig. 2. In this area, the local diffusion coefficient, $D(x,y)$, was reduced using $D(x,y) = D_0 R_d$, where D_0 was the free diffusion coefficient and the reduction factor, R_d, was chosen to be 1 (no reduction effect), 1/4, 1/8, 1/16, and 1/32. It is noted that, if we use eq. (A12) in the numerical simulations on the lattice model shown in Fig. 2, the reduction in the local diffusion coefficient lowers the movement of the TMP not only from the area with this reduction to the outside areas, but also toward this area from the outside areas. The numerical simulations of the master equation given by eq. (A12) were typically performed for 100,000 to 400,000 steps.

IV. Results

To begin with, we show the numerical results for typical cases on the mean square displacement, $\langle r^2(t)\rangle$, obtained from our model (Fig. 3). The red long-dashed line for $p_v = 0.0$ corresponds to the case where the TMP is completely confined inside the initial compartment by the fence obstacles. In this case, $\langle r^2(t)\rangle$ increases with time for a short time after the start time, but it then becomes constant after this, indicating free diffusion early in the process and that it becomes zero diffusion coefficient later on. In the second case with $R_d = 1$ (displayed as the blue dashed line), the stochastic fence effect with the passage probability parameter of $p_v = 0.002$ and the static obstacle effect by the pickets with $p_p = 0.3$ are applied, while the reduction in the local diffusion coefficient around the pickets is not taken into

account. In this case, after the free diffusion at the beginning, $\langle r^2(t)\rangle$ becomes proportional to t^α for $\alpha < 1$ for a while before becoming a linear function of t later on. This observation suggests that a subdiffusion process of the TMP occurs in the intermediate time domain due to the effects by the fence and picket and later on the smooth transition towards normal diffusion takes place after that due to hop diffusion among adjacent compartments. The third case where $p_v = 0.002$, $p_p = 0.3$, and $R_d = 1/32$ (displayed as the black solid line), exhibits an additional subdiffusion process followed by a transient process towards normal diffusion on the late stages of the process. This result is in good agreement with the experimental observations on the TMP diffusion in NRK cell membranes [19] that will be shown in Fig. 4. The difference between the second and third cases, that is, the reduction in the local diffusion coefficient by $R_d = 1/32$, seems to be crucial for the second subdiffusion behavior later in this process. In contrast, the transient process from the free diffusion at the beginning towards the first subdiffusion behavior is attributable to the obstacle effects caused by the fences and pickets.

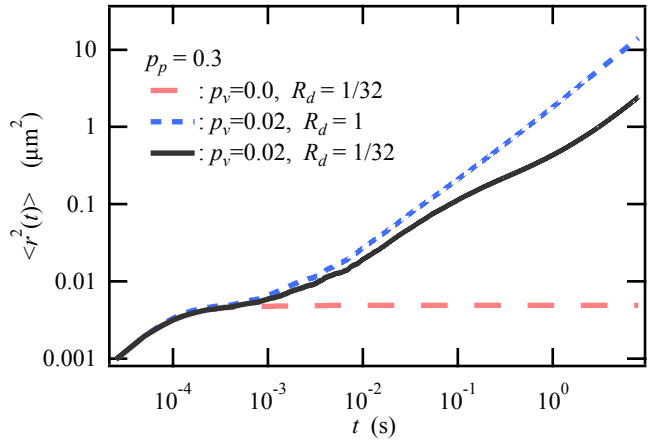

Figure 3. Numerical results for the mean square displacement, $\langle r^2(t)\rangle$, as a function of time, t, for the probability of the picket, $p_p = 0.3$. The result of $\langle r^2(t)\rangle$ with $p_v = 0.002$ and $R_d = 1/32$ agrees well with the experimental data for the μOR in NRK cell membranes [19] shown in Fig. 4.

Next, in order to clarify effects of the reduction in the local diffusive movement around the pickets, we show in Fig. 4 a comparison of the mean square displacements divided by time t, $\langle r^2(t)\rangle/t$, between the experimental data for the μOR in NRK cell membranes [19] (indicated by the blue open circles) and the numerical results obtained at several reduction factors on the local diffusion coefficient around the pickets ($R_d = 1,\ 1/4, 1/8, 1/16,$ and $1/32$) under $p_v = 0.002$ and $p_p = 0.3$. Additionally, the result of $\langle r^2(t)\rangle/t$ for $p_v = 0.002$ and $R_d = 1$ without pickets (i.e. for $p_p = 0.0$), is also shown as the blue solid line in Fig. 4; it is because, this enables us to observe the obstacle effect due to only the pickets in comparing with that for $p_v = 0.002$ and $R_d = 1$ having pickets with $p_p = 0.3$ (red dot-dashed line). We find that all the results of $\langle r^2(t)\rangle/t$ near the beginning of the process (t <10^{-3} s) overlap with each other. The plateau of $\langle r^2(t)\rangle/t$ until 10^{-4} s indicates the free diffusion process of the TMP inside the initial compartment partitioned by the membrane-skeleton fences. This plateau is followed by a decrease in $\langle r^2(t)\rangle/t$ with a negative slope $\alpha - 1$ for $\alpha < 1$ defined by Eq. (A16), indicating that there is a subdiffusion process of the TMP after that; this is believed to have been caused by the compartmentalization with the diameter of 210 nm on average caused by the membrane-skeleton fences. The subdiffusion process for $p_p = 0.0$ (i.e., no pickets) most quickly relaxes toward normal diffusion among these results, so that $\langle r^2(t)\rangle/t$ becomes constant until 0.1 s (see the blue solid line). The constant value of $\langle r^2(t)\rangle/t$ when divided by 4 corresponds to the diffusion coefficient at normal diffusion. In the case where $p_p = 0.3$ and $R_d = 1$ (the red dot-dashed line), more than 1 s is required in order for normal diffusion to occur, and this normal diffusion coefficient is decreased by the addition of the pickets. However, even if we take into account

only the static obstacle effect due to the pickets into consideration along with the stochastic fence effect, we are unable to describe the two-step subdiffusion behavior observed in the experiments. The remaining deviation from the experimental $\langle r^2(t)\rangle/t$ can be significantly reduced by taking into account the decrease in the local diffusivity of the TMP around the pickets. We find that there is a good agreement with the experimental data when the reduction factor of $R_d = 1/32$ is applied to the local diffusion coefficient (the black solid line), which means that $\langle r^2(t)\rangle/t$ for the wide time period including the two-step subdiffusion behavior can be quantitatively described by the present model. The first subdiffusion behavior on $\langle r^2(t)\rangle/t$ at the time between 0.01 s and 0.1 s provided by $R_d = 1/4$ is almost the same as that provided by $R_d = 1/32$, whereas the second subdiffusion behavior later in this process (t >0.1 s) cannot be satisfactorily described by $R_d = 1/4$. The large lowing in the local diffusivity of the TMP around the pickets mainly affects the decrease in the normal diffusion coefficient on the late stages of the process.

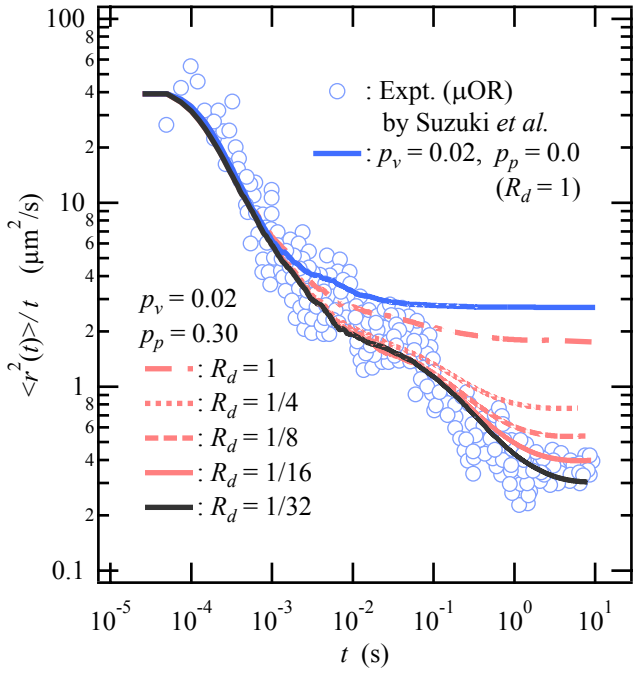

Figure 4. Comparison of the mean square displacements divided by time, $\langle r^2(t)\rangle/t$, between the experimental data for the μOR in NRK cell membranes [19] (blue open circles) and the numerical results obtained at several reduction factors on the local diffusion coefficient around the pickets ($R_d = 1,\ 1/4, 1/8, 1/16,$ and $1/32$) under $p_v = 0.002$ and $p_p = 0.3$. To observe the obstacle effect caused by the pickets, the numerical result for $p_v = 0.002$, $R_d = 1$, and $p_p = 0.0$ (i.e., without pickets) is also displayed as the solid blue line.

As seen in Fig. 4, the effect of the decrease in the local diffusivity around the pickets does not influence $\langle r^2(t)\rangle/t$ early in the process (t <1 ms) that corresponds to the free diffusion and the first subdiffusion process following it, while it does strongly affect the behavior of the TMP diffusion on the latter half of the process that includes the first and second relaxations toward the quasi-normal diffusion and the normal diffusion, respectively. Next, we investigate how the stochastic fence effect influences the diffusion dynamics of the TMP. Here, we do this by varying the passage probability parameter, p_v, under fixing p_p and R_d. Figure 5 shows $\langle r^2(t)\rangle/t$ at several passage probability parameters, $p_v = 1, 0.1, 0.04, 0.02, 0.005,$ and 0, under using the constant parameters for $p_p = 0.3$ and $R_d = 1/32$. $p_v = 1$ and $p_v = 0$ correspond to the conditions without the fence obstacles and with the static fence obstacles that completely prohibit passing the fence lines, respectively. The experimental data[19] is also depicted as blue open circles. The numerical result for $p_v = 0.02$ (indicated by black solid line) is the same as that shown in Fig. 4. The result of $\langle r^2(t)\rangle/t$ for $p_v = 0$ (red solid line) almost overlaps with that for $p_v = 0.02$ early on (t <0.001 s), but it continues to decrease monotonically along with time; that is because of the complete confinement of the TMP within the initial compartment. Therefore, the subdiffusion behavior that is observed early on in all the cases, except for $p_v = 1$ (indicated by the solid blue line), is attributable to the effect of the fence obstacles. In fact, in the case where there are no fence obstacles ($p_v = 1$), no rapid decrease is observed on $\langle r^2(t)\rangle/t$ after the free diffusion, and instead the

subdiffusion behavior with a large negative slope appears at time between 0.01 and 0.1 s. These results imply that the effects of the picket obstacles and/or the decrease in the local diffusivity around the pickets affect the subdiffusion behavior especially on the latter half of the process. As the stochastic obstacle effect increases, the subdiffusion behaviors seen as the rapid decrease in $\langle r^2(t)\rangle/t$ after the free diffusion are observed, and the first and second plateaus become visibly lower. In addition, the timings of the first and second relaxations towards the quasi-normal-diffusion and normal-diffusion processes, respectively, that is, the transition points from a subdiffusion process to a plateau region, gradually shift to be the late stage of the process along with the passage probability parameter p_v. These observations imply that the stochastic fence effect influences the overall diffusion processes for the entire time domain of the process as well.

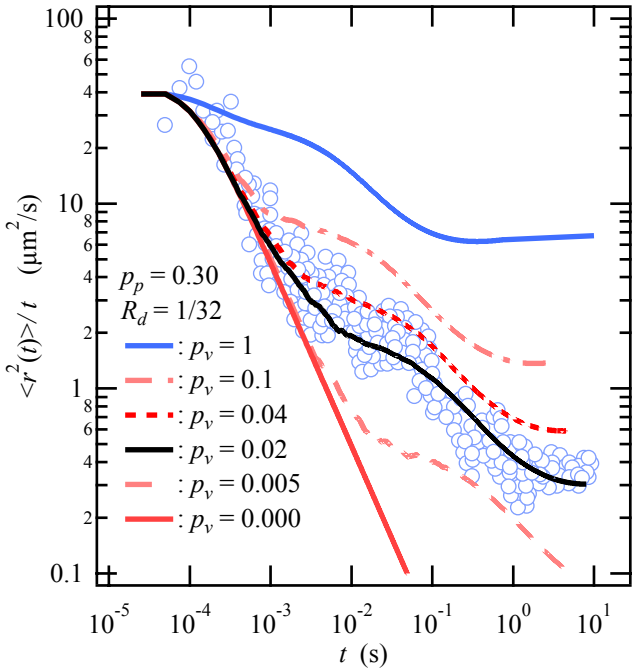

Figure 5. The mean square displacements divided by time, $\langle r^2(t)\rangle/t$, at various passage probability parameters, $p_v = 1, 0.1, 0.04, 0.02, 0.005,$ and 0, under fixing $p_p = 0.3$ and $R_d = 1/32$. Here $p_v = 1$ and $p_v = 0$ correspond to the conditions

without the fence obstacles and with the static fence obstacles that completely prohibit passing the fence lines, respectively. The open blue circles represent the same experimental data as that shown in Fig. 4[19].

Lastly, we examine the effect of the picket concentration dependence on $\langle r^2(t)\rangle/t$ under fixing the parameters for both the probability of the fence obstacles and the decrease in the local diffusivity around the pickets ($p_v = 0.02$ and $R_d = 1/32$) (see Fig. 6). Note that the area in which the local diffusivity decreases due to the pickets also increases according to the increase in the probability of the picket. Similar to that seen in Fig. 4, the rapid decreases in $\langle r^2(t)\rangle/t$ early in the process (t <1 ms) overlap one another for all values of p_p (Fig. 6), indicating that the combination of the picket obstacle and the decrease in the local diffusivity does not affect the short-time behavior of the TMP diffusion. The second subdiffusion behavior becomes notable, as seen in Fig. 4, and not only does the second plateau decrease, but so does the first plateau, when the probability of the picket p_p increases; furthermore, the increase in p_p more strongly reduces the second plateau on the late stage of the process.

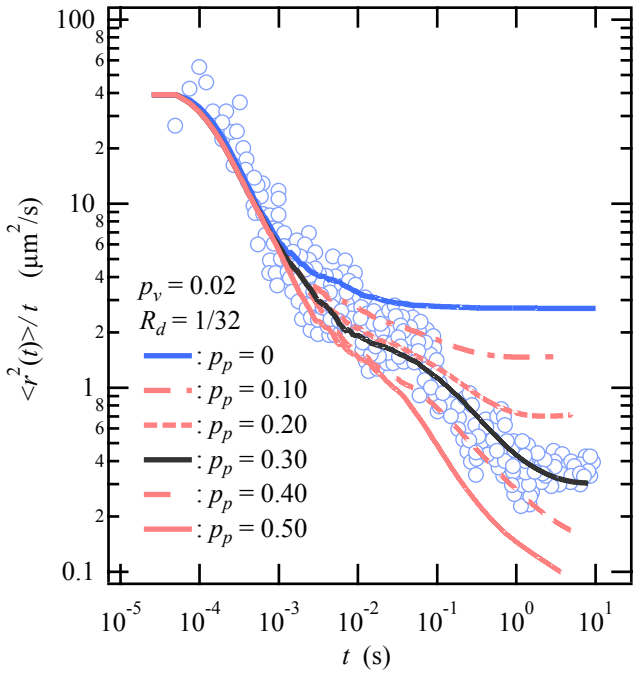

Figure 6. The mean square displacements divided by time, $\langle r^2(t)\rangle/t$, at various picket probabilities ($p_p = 0, 0.1, 0.2, 0.3, 0.4, \text{and } 0.5$) under fixing the parameters for both the probability of the stochastic fence obstacle and the decrease in the local diffusivity around the pickets ($p_v = 0.02$ and $R_d = 1/32$). Notably, the area in which the local diffusivity is decreased by $R_d = 1/32$ is increased according to the increase in p_p. The open blue circles indicate the same experimental data as that shown in Figs. 4 and 5[19].

V. Discussion

Fujiwara *et al*. proposed the model for NRK cell membranes based on nested double compartments in order to explain the two different values that they determined for the diffusion coefficient of the unsaturated phospholipid, DOPE (and transferrin receptor, TfR) [14]. Suzuki *et al*. also used the same model to explain the two-step subdiffusion behavior of the TMP, μOR, that they observed in NRK plasma membranes [19]. They pointed out that the anchored-membrane-protein picket and/or the membrane-skeleton fence temporally confined the DOPE and TMP within

the nested double compartments. However, even if the two different boundaries that are responsible for the nested double compartmentalization are easily molded assuming high and low energy barriers as Fujiwara *et al.* pointed out, it has been remained unclear how the two different boundaries can be explained on the basis of the fence and picket. Sung and Yethiraj performed Monte Carlo simulations of TMP diffusion according to the nested double compartment model[30]. They modeled the fences as obstacle particles and used them to form the large compartments. In addition, they modeled the small compartments by randomly distributing attractive traps at a specific concentration to the plasma membrane. Their model quantitatively described the experimental $\langle r^2(t)\rangle/t$ of the TMP. In contrast to their model, we did not explicitly introduce large compartments, while we assumed that the fences and pickets were responsible for forming the small compartments. Instead of the nested double compartments, to describe the two-step subdiffusion behavior in $\langle r^2(t)\rangle/t$, we introduced dynamic heterogeneity, that is, a decrease in the local diffusivity of the TMP around the pickets bound to the membrane-cytoskeleton fences. Possible explanation of the physical origin on the decrease in the local diffusivity of the TMP is based on an increase in the viscous friction caused by the reduction in the diffusive movement of the phospholipid molecules around the picket proteins; in fact, such significant reduction has been remarkably observed at the axonal initial segment in plasma membrane of developing hippocampal neurons in culture[37].

It has been demonstrated that the relaxation from subdiffusion to normal diffusion caused by stochastic (dynamical or mobile) obstacle effects, such as the fence effect, is much faster than that caused by static (immobile) obstacle effects such as the picket effects[38], even if the concentration of the stochastic obstacles is, for instance, ten

times higher than that of the static ones. This is because the relaxation of a non-Gaussian distribution caused by the stochastic obstacles towards a steady-state Gaussian distribution is notably faster than that caused by the static obstacles. The subdiffusion behaviors that have commonly been observed in previous studies in the presence of static and/or stochastic obstacles are qualitatively consistent with the results obtained from our model: the subdiffusion process caused by the fences acting as the stochastic obstacles is observed at the time domain much earlier than by both the immobile picket obstacles and the decrease in the local diffusivity around the pickets. Thus the latter effects are considered to have the static retarding effect on the TMP diffusion. The two-step subdiffusion behavior is attributable to the different timescales in the relaxation of subdiffusion towards normal diffusion due to those static and stochastic obstacle effects.

VI. Summary

In the present study, we performed two-dimensional lattice simulations of the master equation using the simple plasma membrane model in order to investigate the mechanism of the two-step subdiffusion behavior on lateral movement of the TMP, which had previously been experimentally observed as being heterogeneous diffusion dynamics of the μ-opioid receptor (μOR) in NRK cell membranes. It had been found that the μOR was temporarily confined within compartments and after a while underwent hop diffusion among the membrane compartments [19]. It had been proposed that the membrane compartments were delimited by both the membrane-skeleton fence and the anchored-membrane-protein picket[14,19]. The former and the latter can be considered to be stochastic (dynamical) and static (immobile) obstacles on the diffusion process, respectively.

At first, we examined a simple model that is only consisted of fences and pickets. We found that this model exhibited not the two-step subdiffusion process, but only a simple single-step subdiffusion behavior. Our result is consistent with the claim by Meilhac *et al*. [39]: the long-term normal diffusion cannot be explained by only the fence and picket models; thus, another mechanism must be introduced to explain the long-term normal diffusion [40]. Following this preliminary study, we examined the combination model, where we took into account a decrease in the local diffusivity of the TMP around the pickets in addition to the effects caused by the fences and pickets. Here, we assumed that the decrease in the TMP's local diffusivity was due to a decrease in the local diffusivity of phospholipid molecules around anchored-protein pickets, which had previously been observed at an axonal initial segment in plasma membranes of developing hippocampal neurons in culture [37]. The fence and picket models, combined with the decrease in the local diffusion coefficient of the TMP around the pickets, quantitatively described the two-step subdiffusion behavior as seen in the mean square displacement divided by time, $\langle r^2(t)\rangle/t$, when the compartments with the diameter of 210 nm were assumed to be delimited by the membrane-skeleton fences. By varying the parameters, namely, the probability of the TMP passage across the fences, p_v, the coverage parameter of the anchored-membrane-protein pickets along the fences, p_p, and the reduction factor R_d by which the local diffusion coefficient of the TMP around the pickets is reduced than the free diffusion, we obtained the following results. (1) No two-step subdiffusion behavior can be described either by only the fence effect or by only the picket effect combined with the decrease in the local diffusivity of the TMP around the pickets. (2) The effect due to the decrease in the local diffusivity under fixing the parameters for p_v and p_p particularly decreases the normal diffusion coefficient related to

the final stage of the diffusion process. (3) The effect caused by the decrease in the stochastic passage probability parameter p_v under the constant values for p_p and R_d results in the slowing down of the diffusive dynamics as well and as a consequence shifts whole the timings in the diffusion process to be later on. (4) The increase in the picket concentration and the increase in the local diffusivity provide the similar effect on the TMP's diffusion dynamics; that is, the decrease in $\langle r^2(t)\rangle/t$ at time greater than 1 ms and no influence on the first subdiffusion behavior at time shorter than it. (5) The experimentally observed two-step subdiffusion behavior is attributable to the different timescales in the relaxation of subdiffusion towards normal diffusion; the relaxation of the subdiffusion caused by the static retarding effect due to both the picket obstacles and inhomogeneous reduction in the local diffusivity is obviously slower than that caused by the stochastic obstacle effect due to the fences.

Insights into the diffusion dynamics of the TMP gaining by the present study are twofold; firstly, two different length scales, such as those characterized by nested double compartments, are not necessarily needed to describe the two-step subdiffusion processes observed at the different time domains; secondly, the two-step subdiffusion behavior can be also described by the combination of the hop diffusion, which is due to single-size small compartments, and the heterogeneous diffusion dynamics of the TMP caused by the decrease in the local diffusivity of phospholipid molecules. In our group, a detrended fluctuation analysis (DFA)[41] is being applied to characterize the fluctuation of time series on random walk trajectories that describe similar two-step subdiffusion behavior obtained from Monte Carlo simulations

[42]. The DFA analysis would be useful to analyze the fractal properties to be inherent in actual time series data on the trajectory observed by singe-particle tracking for TMP and lipid.

Acknowledgments

This work was supported by the Grants-in-Aid for Scientific Research (KAKENHI) from the Ministry of Education, Culture, Sports, Science and Technology of Japan. We would like to thank Professor Tsuyoshi Yamaguchi at Nagoya University for useful suggestion on the derivation of the discrete-time master equation based on the diffusion equation in inhomogeneous media. We would also like to thank Dr. Yoshinobu Tanaka, Mr. Shotaro Okuda, and Mr. Tomoshige Ishii for performing preliminary calculations of the master equation. Finally, T.S. would like to thank Dr. Ryuichi Okamoto in Okayama University for appropriate comments on revising the manuscript.

APPENDIX

To perform the numerical simulations for the diffusion process of the TMP in the two-dimensional lattice model of the plasma membrane, we use a discrete-time master equation in two dimensions that can be obtained from a diffusion equation in inhomogeneous medium (for instance, Refs. [43,44]). The diffusion equation is obtained from the continuity equation and Fick's first law (Eqs. (A1) and (A2), respectively):

$$\frac{\partial P(x,y,t)}{\partial t} = -\nabla \cdot \boldsymbol{J}(x,y,t) \tag{A1}$$

$$\boldsymbol{J}(x,y,t) = -\boldsymbol{D}(x,y)\nabla \boldsymbol{P}(x,y,t), \tag{A2}$$

where $\boldsymbol{P(x,y,t)}$ is the probability density of finding a diffusion particle at a position $\boldsymbol{(x,y)}$ at time *t*, $\boldsymbol{J(x,y,t)}$ is the flux of $\boldsymbol{P(x,y,t)}$, and $\boldsymbol{D(x,y)}$ is the diffusion coefficient varying in space. By substituting Eq. (A2) into Eq. (A1), we obtain generalization of the diffusion equation for an inhomogeneous medium:

$$\frac{\partial P(x,y,t)}{\partial t} = \frac{\partial}{\partial x}\left[D(x,y)\frac{\partial}{\partial x}P(x,y,t)\right] + \frac{\partial}{\partial y}\left[D(x,y)\frac{\partial}{\partial y}P(x,y,t)\right]. \tag{A3}$$

Next, we apply the following approximation for the partial differentiations of Eq. (A3):

$$\frac{\partial}{\partial x}f(x,y,t) = \frac{f(x+\Delta x/2,y,t)-f(x-\Delta x/2,y,t)}{\Delta x} + O(\Delta x^2), \tag{A4}$$

after which we obtain the following equation:

$$\begin{aligned}\frac{\partial P(x,y,t)}{\partial t} = {} & \frac{1}{\Delta x}\left[D\left(x+\frac{\Delta x}{2},y\right)\frac{\partial}{\partial x}P\left(x+\frac{\Delta x}{2},y,t\right)\right] - \frac{1}{\Delta x}\left[D\left(x-\frac{\Delta x}{2},y\right)\frac{\partial}{\partial x}P\left(x-\frac{\Delta x}{2},y,t\right)\right] \\ & + \frac{1}{\Delta y}\left[D\left(x,y+\frac{\Delta y}{2}\right)\frac{\partial}{\partial y}P\left(x,y+\frac{\Delta y}{2},t\right)\right] - \frac{1}{\Delta y}\left[D\left(x,y-\frac{\Delta y}{2}\right)\frac{\partial}{\partial y}P\left(x,y-\frac{\Delta y}{2},t\right)\right].\end{aligned} \tag{A5}$$

By applying Eq. (A4) to the partial differentiations in Eq. (A5), we obtain the following equation:

$$\begin{aligned}\frac{\partial P(x,y,t)}{\partial t} = {} & \frac{1}{\Delta x}\left[D\left(x+\frac{\Delta x}{2},y\right)\frac{1}{\Delta x}\left(P(x+\Delta x,y,t)-P(x,y,t)\right)\right] \\ & - \frac{1}{\Delta x}\left[D\left(x-\frac{\Delta x}{2},y\right)\frac{1}{\Delta x}\left(P(x,y,t)-P(x-\Delta x,y,t)\right)\right] \\ & + \frac{1}{\Delta y}\left[D\left(x,y+\frac{\Delta y}{2}\right)\frac{1}{\Delta y}\left(P(x,y+\Delta y,t)-P(x,y,t)\right)\right] \\ & - \frac{1}{\Delta y}\left[D\left(x,y-\frac{\Delta y}{2}\right)\frac{1}{\Delta y}\left(P(x,y,t)-P(x,y-\Delta y,t)\right)\right].\end{aligned} \tag{A6}$$

If we then apply the following approximation for the partial differentiation with respect to *t* to Eq. (A6):

$$\frac{\partial}{\partial t} f(x,y,t) = \frac{f(x,y,t+\Delta t) - f(x,y,t)}{\Delta t} + O(\Delta t), \tag{A7}$$

we obtain the following equation:

$$\boldsymbol{P(x,y,t+\Delta t)} = \left[\mathbf{1} - \frac{\boldsymbol{\Delta t D(x+\Delta x/2,y)}}{\boldsymbol{\Delta x^2}} - \frac{\boldsymbol{\Delta t D(x-\Delta x/2,y)}}{\boldsymbol{\Delta x^2}} - \frac{\boldsymbol{\Delta t D(x,y+\Delta y/2)}}{\boldsymbol{\Delta y^2}} - \frac{\boldsymbol{\Delta t D(x,y-\Delta y/2)}}{\boldsymbol{\Delta y^2}}\right] \boldsymbol{P(x,y,t)}$$

$$+ \frac{\boldsymbol{\Delta t D(x+\Delta x/2,y)}}{\boldsymbol{\Delta x^2}} \boldsymbol{P(x+\Delta x,y,t)} + \frac{\boldsymbol{\Delta t D(x-\Delta x/2,y)}}{\boldsymbol{\Delta x^2}} \boldsymbol{P(x-\Delta x,y,t)}$$

$$+ \frac{\boldsymbol{\Delta t D(x,y+\Delta y/2)}}{\boldsymbol{\Delta y^2}} \boldsymbol{P(x,y+\Delta y,t)} + \frac{\boldsymbol{\Delta t D(x,y-\Delta y/2)}}{\boldsymbol{\Delta y^2}} \boldsymbol{P(x,y-\Delta y,t)}. \tag{A8}$$

To eliminate $\Delta x/2$ and $\Delta y/2$ from Eq. (A8), we apply the following approximation:

$$\boldsymbol{D(x+\Delta x/2,y)} = \big(\boldsymbol{D(x,y)} + \boldsymbol{D(x+\Delta x,y)}\big)/\mathbf{2} \tag{A9}$$

to Eq. (A8). This enables us to obtain the following equation:

$$\boldsymbol{P(x,y,t+\Delta t)} = \left[\mathbf{1} - \frac{\boldsymbol{D(x+\Delta x,y)+D(x,y)}}{\mathbf{10}\boldsymbol{D_0}} - \frac{\boldsymbol{D(x,y)+D(x-\Delta x,y)}}{\mathbf{10}\boldsymbol{D_0}} - \frac{\boldsymbol{D(x,y+\Delta y)+D(x,y)}}{\mathbf{10}\boldsymbol{D_0}} - \frac{\boldsymbol{D(x,y)+D(x,y-\Delta y)}}{\mathbf{10}\boldsymbol{D_0}}\right] \boldsymbol{P(x,y,t)}$$

$$+ \frac{\boldsymbol{D(x+\Delta x,y)+D(x,y)}}{\mathbf{10}\boldsymbol{D_0}} \boldsymbol{P(x+\Delta x,y,t)} + \frac{\boldsymbol{D(x,y)+D(x-\Delta x,y)}}{\mathbf{10}\boldsymbol{D_0}} \boldsymbol{P(x-\Delta x,y,t)}$$

$$+ \frac{\boldsymbol{D(x,y+\Delta y)+D(x,y)}}{\mathbf{10}\boldsymbol{D_0}} \boldsymbol{P(x,y+\Delta y,t)} + \frac{\boldsymbol{D(x,y)+D(x,y-\Delta y)}}{\mathbf{10}\boldsymbol{D_0}} \boldsymbol{P(x,y-\Delta y,t)}, \tag{A10}$$

where $\Delta t = \Delta x^2/5D_0$ and $\Delta t = \Delta y^2/5D_0$ are used in Eq. (A10) to obtain this simple loss-and-gain-type equation governing $P(x,y,t)$. In fact, if $D(x,y)$ is always equal to D_0, then Eq. (A10) can be reduced to the following equation:

$$\boldsymbol{P(x,y,t+\Delta t)} = \frac{\mathbf{1}}{\mathbf{5}}[\boldsymbol{P(x,y,t)} + \boldsymbol{P(x+\Delta x,y,t)} + \boldsymbol{P(x-\Delta x,y,t)} + \boldsymbol{P(x,y+\Delta y,t)} + \boldsymbol{P(x,y-\Delta y,t)}], \tag{A11}$$

which corresponds to the master equation obtained from the diffusion equation for homogeneous mediums. An extension of Eq. (A10) that takes into account obstacle effects is subsequently straightforward, as demonstrated in Eq. (A12):

$$\boldsymbol{P(x,y,t+\Delta t) = P(x,y,t) + \frac{D(x+\Delta x,y)+D(x,y)}{10D_0} P(x+\Delta x,y,t)e(x,y) + \frac{D(x,y)+D(x-\Delta x,y)}{10D_0} P(x-\Delta x,y,t)e(x,y)}$$

$$\boldsymbol{+ \frac{D(x,y+\Delta y)+D(x,y)}{10D_0} P(x,y+\Delta y,t)e(x,y) + \frac{D(x,y)+D(x,y-\Delta y)}{10D_0} P(x,y-\Delta y,t)e(x,y)}$$

$$- \frac{D(x+\Delta x,y)+D(x,y)}{10D_0} P(x,y,t)e(x+\Delta x,y) - \frac{D(x,y)+D(x-\Delta x,y)}{10D_0} P(x,y,t)e(x-\Delta x,y)$$

$$- \frac{D(x,y+\Delta y)+D(x,y)}{10D_0} P(x,y,t)e(x,y+\Delta y) - \frac{D(x,y)+D(x,y-\Delta y)}{10D_0} P(x,y,t)e(x,y-\Delta y), \quad \text{(A12)}$$

where $e(x,y)$ is provided by the following relationship:

$$e(x,y) = \begin{cases} 1, & (x,y) \neq \Omega \\ 0, & (x,y) = \Omega, \end{cases} \quad \text{(A13)}$$

where Ω indicates a set of lattice sites occupied by obstacles, namely, the fence and picket obstacles. The numerical simulation is started from an initial site, (x_0, y_0). The mean square displacement at time *t* is calculated using the following equation:

$$\langle r^2(t) \rangle = \sum_{x_k} \sum_{y_l} \{(x_k - x_0)^2 + (y_l - y_0)^2\} P(x_k, y_l, t). \quad \text{(A14)}$$

When the diffusion process reaches the steady state after enough time has passed, $\langle r^2(t) \rangle$ becomes a linear function of time *t*, as shown below:

$$\langle r^2(t) \rangle = C + 4Dt, \quad \text{(A15)}$$

where D is the diffusion coefficient for the steady state and C is a constant that depends on the initial state. However, during a transient process toward the steady state, that is, a subdiffusion process, $\langle r^2(t)\rangle$ scales with time *t* as $\langle r^2(t)\rangle \sim t^{\alpha}$ with $\alpha < 1$. As such, we can use $\langle r^2(t)\rangle/t$ to characterize the diffusion process:

$$\langle r^2(t)\rangle/t \sim \begin{cases} t^{\alpha-1} & \text{subdiffusion } (\alpha - 1 < 0) \\ \text{constant} & \text{normal diffusion.} \end{cases} \tag{A16}$$

In the subdiffusion, $\boldsymbol{\langle r^2(t)\rangle/t}$ is a function of time $\boldsymbol{t}$. We can use Eq. (A15) to determine the diffusion coefficient, $\boldsymbol{D}$, for the steady state. When $\boldsymbol{\langle r^2(t)\rangle/4t}$ is in proximity to the steady state, it should approach $\boldsymbol{D}$ in proportion to $\boldsymbol{1/t}$ as $\boldsymbol{t}$ increases, because of $\boldsymbol{\langle r^2(t)\rangle/4t = C/4t + D}$ that is outlined in Eq. (A15). Using the asymptotic behavior of $\boldsymbol{\langle r^2(t)\rangle/4t}$ as a function of $\boldsymbol{1/t}$, we can determine the diffusion coefficient $\boldsymbol{D}$ at the steady state with a high degree of accuracy, although we do not discuss the value of $\boldsymbol{D}$ at the steady state in the present study.

The obtained master equation Eq. (A10) can reproduce the accurate result of $\boldsymbol{\langle r^2(t)\rangle}$ provided by the diffusion equation Eq. (A3), if $\boldsymbol{\Delta x}$ and $\boldsymbol{\Delta y}$ used in the numerical simulations are sufficiently small compared with the spatial variation of $\boldsymbol{D(x,y)}$. On the other hand, in the present study, we apply Eq. (A13)–which is an extension of Eq. (A10) by considering obstacles–to the lattice model shown in Fig. 2. In our preliminary calculations, we confirmed that the numerical simulations by Eq. (A13) accurately reproduced the result of $\boldsymbol{\langle r^2(t)\rangle}$ provided by Monte Carlo simulations of random walk under considering the fence and picket obstacles.

REFERENCES

[1] S. J. Singer and G. L. Nicolson, Science **175**, 720 (1972).

[2] M. P. Sheetz, M. Schindler, and D. E. Koppel, Nature **285**, 510 (1980).

[3] C.-H. CHANG, H. TAKEUCHI, T. ITO, K. MACHIDA, and S.-I. OHNISHI, J Biochem **90**, 997 (1981).

[4] G. Lindblom, L. Johansson, and G. Arvidson, Biochemistry **20**, 2204 (1981).

[5] R. PETERS and R. J. CHERRY, Proc. Natl. Acad. Sci. U.S.a. **79**, 4317 (1982).

[6] M. Swaisgood and M. Schindler, Experimental Cell Research **180**, 515 (1989).

[7] G. M. LEE, J. Cell Biol. **120**, 25 (1993).

[8] S. Ladha, P. S. James, D. C. Clark, E. A. Howes, and R. Jones, Journal of Cell Science **110**, 1041 (1997).

[9] G. J. Schütz, G. Kada, V. P. Pastushenko, and H. Schindler, Embo J **19**, 892 (2000).

[10] D. E. Golan and W. Veatch, Proc. Natl. Acad. Sci. U.S.a. **77**, 2537 (1980).

[11] A. Tsuji and S. Ohnishi, Biochemistry **25**, 6133 (1986).

[12] A. Tsuji, K. Kawasaki, S. Ohnishi, and H. Merkle, Biochemistry **27**, 7447 (1988).

[13] N. Destainville, A. Saulière, and L. Salomé, Biophys. J. **95**, 3117 (2008).

[14] T. Fujiwara, K. Ritchie, H. Murakoshi, K. Jacobson, and A. Kusumi, J. Cell Biol. **157**, 1071 (2002).

[15] A. Kusumi, Y. Sako, and M. Yamamoto, Biophys. J. **65**, 2021 (1993).

[16] Y. Sako and A. Kusumi, J. Cell Biol. **125**, 1251 (1994).

[17] Y. Sako and A. Kusumi, J. Cell Biol. **129**, 1559 (1995).

[18] M. Tomishige, Y. Sako, and A. Kusumi, J. Cell Biol. **142**, 989 (1998).

[19] K. Suzuki, K. Ritchie, E. Kajikawa, T. Fujiwara, and A. Kusumi, Biophysical Journal **88**, 3659 (2005).

[20] M. J. Saxton, Biophysical Journal **55**, 21 (1989).

[21] M. J. Saxton, Biophysical Journal **56**, 615 (1989).

[22] M. J. Saxton, Biophys. J. **57**, 1167 (1990).

[23] M. J. Saxton, Biophysical Journal **66**, 394 (1994).

[24] M. J. Saxton, Biophys. J. **69**, 389 (1995).

[25] M. J. Saxton, Biophys. J. **70**, 1250 (1996).

[26] M. J. Saxton and K. Jacobson, Annu Rev Biophys Biomol Struct **26**, 373 (1997).

[27] B. J. Sung and A. Yethiraj, Phys. Rev. Lett. **96**, 228103 (2006).

[28] M. J. Saxton, Biophys. J. **92**, 1178 (2007).

[29] B. J. Sung and A. Yethiraj, J Phys Chem B **112**, 143 (2008).

[30] B. J. Sung and A. Yethiraj, Biophys. J. **97**, 472 (2009).

[31] H. Li, Y. Zhang, V. Ha, and G. Lykotrafitis, Soft Matter **12**, 3643 (2016).

[32] L. A. Gheber and M. Edidin, Biophys. J. **77**, 3163 (1999).

[33] F. Brown, D. M. Leitner, J. A. McCammon, and K. R. Wilson, Biophys. J. **78**, 2257 (2000).

[34] Z. Kalay, P. E. Parris, and V. M. Kenkre, J. Phys.: Condens. Matter **20**, 245105 (2008).

[35] V. M. Kenkre, L. Giuggioli, and Z. Kalay, Phys. Rev. E **77**, 051907 (2008).

[36] T. Auth and N. S. Gov, Biophys. J. **96**, 818 (2009).

[37] C. Nakada, K. Ritchie, Y. Oba, M. Nakamura, Y. Hotta, R. Iino, R. S. Kasai, K. Yamaguchi, T. Fujiwara, and A. Kusumi, Nat Cell Biol **5**, 626 (2003).

[38] M. J. Saxton, Biophys. J. **52**, 989 (1987).

[39] N. Meilhac, L. Le Guyader, L. Salomé, and N. Destainville, Phys. Rev. E **73**, 011915 (2006).

[40] F. Daumas, N. Destainville, C. Millot, A. Lopez, D. Dean, and L. Salomé, Biophys. J. **84**, 356 (2003).

[41] C. K. Peng, S. V. Buldyrev, A. L. Goldberger, S. Havlin, F. Sciortino, M. Simons, and H. E. Stanley, Nature **356**, 168 (1992).

[42] A. Okumoto, T. Sumi, H. Sekino, and H. Goto, Journal of Computer Chemistry, Japan **15**, 229 (2017).

[43] N. G. van Kampen, Zeitschrift Für Physik B Condensed Matter **68**, 135 (1987).

[44] N. G. van Kampen, Journal of Physics and Chemistry of Solids **49**, 673 (1988).